Geophysical Prospecting, 2007, **55**, 255–264

A derivative-based interpretation approach to estimating source parameters of simple 2D magnetic sources from Euler deconvolution, the analytic-signal method and analytical expressions of the anomalies

Wen-Bin Doo, Shu-Kun Hsu* and Yi-Ching Yeh

Institute of Geophysics, National Central University, Taiwan

Received January 2006, revision accepted July 2006

ABSTRACT

The major advantage of using either the analytic-signal or the Euler-deconvolution technique is that we can determine magnetic-source locations and depths independently of the ambient earth magnetic parameters. In this study, we propose adopting a joint analysis of the analytic signal and Euler deconvolution to estimate the parameters of 2D magnetic sources. The results can avoid solution bias from an inappropriate magnetic datum level and can determine the horizontal locations, depths, structural types (indices), magnetization contrasts and/or structural dips. We have demonstrated the feasibility of the proposed method on 2D synthetic models, such as magnetic contacts (faults), thin dikes and cylinders. However, the method fails to solve the parameters of magnetic sources if there is severe interference between the anomalies of two adjacent magnetic sources.

INTRODUCTION

The analytic-signal and the Euler-deconvolution techniques have been widely used for estimating subsurface magnetic or gravity source parameters (e.g. Nabighian 1972, 1974, 1984; Thompson 1982; Reid *et al*. 1990; Roest *et al*. 1992; Hsu *et al*. 1996; Thurston and Smith 1997; Hsu *et al*. 1998; Smith *et al*. 1998; Fedi and Florio 2001; Salem and Ravat 2003; Williams *et al*. 2005; Smith and Salem 2005). The main advantage of using these two techniques is that we can delineate geological boundaries and determine depths to sources without considering the ambient earth magnetic parameters. However, in the traditional Euler-deconvolution method, an a *priori* selected structural index is usually used to estimate the causative source position (Thompson 1982). The relationship between the structural index and the geometry of the causative body is shown in Table 1. Unfortunately, the geometric type of a subsurface magnetic source is also a parameter that a geologist or geophysicist would wish to determine. Moreover, the datum level of a magnetic anomaly usually involved in the traditional Euler-deconvolution method is difficult to determine unambiguously, which results in the dependence of the structural index on the datum level. An incorrect structural index causes spatially diffuse Euler solutions (Thompson 1982; Reid *et al*. 1990; Ravat 1996; Hsu 2002). Salem and Ravat (2003) proposed a combined method (AN-EUL), based on the Euler equation and the analytic signal. Their method is independent of datum level but it can only determine locations and geometry of the causative magnetic sources. Mushayandebvu *et al*. (2001) also proposed using both Euler-deconvolution and analytic-signal techniques to solve the magnetic parameters of 2D models, such as contact and thin-sheet sources. However, the results from their method are still affected by an uncertain datum level and they have to determine the structural type prior to the application of the technique. Hsu (2002) proposed a combined inversion for the structural index and the source locations from Euler's equation by using only the derivatives of the magnetic anomalies. On the basis of Hsu's (2002) method, we propose a joint analysis of the analytic-signal and Euler-deconvolution

*E-mail: hsu@ncu.edu.tw

Table 1 Relationship between structural index (*N*), type of magnetic model and position of the calculated depth (Hsu 2002)

N	Type of magnetic model	Position of Euler depth relative to the model
0	Contact or fault with small depth/throw ratio	At top and edge
1	Thin dike or fault with large depth/throw ratio	At top and centre, or at edge and half throw
2	Vertical or horizontal cylinder	At centre
3	Sphere	At centre

techniques, which allows us to estimate more magnetic parameters of the subsurface source, such as magnetization contrasts and structural dips, in addition to structural types, horizontal locations and depths.

METHOLOGY

Hsu (2002) gave the general formula for Euler's equation as

$$(x-x_0)\frac{\partial}{\partial x}\left(\frac{\partial^n M}{\partial z^n}\right)+(y-y_0)\frac{\partial}{\partial y}\left(\frac{\partial^n M}{\partial z^n}\right)+(z-z_0)\frac{\partial}{\partial z}\left(\frac{\partial^n M}{\partial z^n}\right)=-(N+n)\left(\frac{\partial^n M}{\partial z^n}\right), \quad (1)$$

where $M(x, y, z)$ is the magnetic anomaly caused by a magnetic source at location (x_0, y_0, z_0), N represents one of several magnetic source types as shown in Tables 1, and n is the order of the derivative (zeroth order for the original anomaly). By adopting n greater than zero, the location and type of a magnetic source can be solved without knowledge of the datum level, as long as the regional comprises an appropriate low-order polynomial. However, the higher-order derivatives can be affected by noisy data. In the case of $n = 1$, we can only deal with an anomaly that is located in a low-order polynomial regional field. Equation (1) then becomes

$$(x-x_0)\frac{\partial}{\partial x}\left(\frac{\partial M}{\partial z}\right)+(z-z_0)\frac{\partial}{\partial z}\left(\frac{\partial M}{\partial z}\right)=-(N+1)\frac{\partial M}{\partial z}. \quad (2)$$

In order to determine x_0, z_0 and N, we need $\frac{\partial M}{\partial x}$ and $\frac{\partial M}{\partial z}$ data in equation (2). We can calculate the horizontal derivative of the magnetic anomaly M from magnetic anomaly data, while the vertical derivative of the magnetic anomaly M can be obtained using the Hilbert transform or the analytic signal (e.g. Hsu *et al*. 1996). Equation (2) is used to solve three magnetic parameters (x_0, z_0 and N) in the sense of least-squares error. We can also solve equation (2) by using the exact formula for the vertical derivative of the corresponding magnetic source. By using both the analytic-signal and Euler-deconvolution techniques and solving the analytical expressions for the appropriate geometries (see below), it is possible to estimate additional magnetic parameters of a magnetic source. Here, we demonstrate the approach for magnetic contact, thin-dike and cylinder models.

The case of a contact or fault model

The equations for the total-field magnetic anomaly (M) and its derivatives from a geological contact or fault model are given by Nabighian (1972). The vertical derivative of the magnetic contact model is expressed as

$$\frac{\partial M}{\partial z}=\alpha\frac{(x-x_0)\cos\beta+(z-z_0)\sin\beta}{r^2}. \quad (3)$$

where $\alpha = 2kFc\sin(d)$, $\beta = 2I - d - 90^\circ$ and $r^2 = (x-x_0)^2 + (z-z_0)^2$. The parameter k is the susceptibility contrast, d is the structural dip calculated counterclockwise from a horizontal level, F is the total intensity of the earth's magnetic field, $c = 1 - \cos^2 i \sin^2 A$, where i is the inclination of the earth's magnetic field and A is the angle between magnetic north and the x-axis, and $I = \tan^{-1}[\frac{\tan i}{\cos A}]$. Substituting equation (3) in the right-hand side of equation (2) and using the structural index $N = 0$ (for the case of a magnetic contact), we obtain

$$(x-x_0)\frac{\partial}{\partial x}\left(\frac{\partial M}{\partial z}\right)+(z-z_0)\frac{\partial}{\partial z}\left(\frac{\partial M}{\partial z}\right)=-\alpha\frac{(x-x_0)\cos\beta+(z-z_0)\sin\beta}{r^2}. \quad (4)$$

We can solve for the parameters α and β using equation (4) and the method of least-squares. From that, we can determine the structural dip (d) and the magnetization contrast (kF) if we assume that the magnetic anomaly is induced by a field similar to the present earth's magnetic field.

The case of a thin-dike model

The equation for the total-field magnetic anomaly (M) and its derivatives from a thin dike was given by Mushayandebvu

et al. (2001). The vertical derivative is expressed as

$$\frac{\partial M}{\partial z} = \alpha_{\mathrm{d}}\left\{\frac{-2\,(z-z_0)\,[(x-x_0)\sin\beta-(z-z_0)\cos\beta]}{r^4} - \frac{\cos\beta}{r^2}\right\}, \tag{5}$$

where $\alpha_{\mathrm{d}} = 2kFct\,\sin(d)$ and t is the thickness of the dike. The other parameters have the same definitions as for the magnetic contact. Substituting equation (5) in the right-hand side of equation (2), and using the structural index $N = 1$ (for the case of a thin dike), we obtain

$$(x-x_0)\,\frac{\partial}{\partial x}\left(\frac{\partial M}{\partial z}\right) + (z-z_0)\,\frac{\partial}{\partial x}\left(\frac{\partial M}{\partial z}\right) = 4\alpha_{\mathrm{d}}\,(z-z_0)\,\frac{[(x-x_0)\sin\beta+(z-z_0)\cos\beta]}{r^4} + \frac{2\alpha_{\mathrm{d}}\cos\beta}{r^2}, \tag{6}$$

In the same way as for equation (4), we can solve equation (6) for the parameters α and β in the sense of least-squares. We can also determine the structural dip (d) and the product of the magnetization contrast and dike thickness (i.e. kFt) if we assume that the magnetic anomaly is induced by a field similar to the present earth's magnetic field.

The case of a cylinder model

The equation for the total-field magnetic anomaly (M) of a cylinder model (Murthy and Mishra 1980) is

$$M = \alpha_{\mathrm{c}}\left[\frac{z^2-x^2}{(z^2+x^2)^2}\cos\beta + \frac{2xz}{(z^2+x^2)^2}\sin\beta\right], \tag{7}$$

where $\alpha_{\mathrm{c}} = 2kF_0'S\frac{\sin i}{\sin i'}$, $F_0' = F\frac{\sin i}{\sin i'}$, $i' = \tan^{-1}[\frac{\tan i}{\sin\delta}]$, F is the total-field intensity of the earth's magnetic field, i is the inclination of the earth's magnetic field, δ is the angle between magnetic north and the strike of the magnetic body, S is the cross-sectional area and $\beta = 2i' - 180^\circ$. The vertical derivative of equation (7) can be obtained as

$$\frac{\partial M}{\partial z} = \alpha_{\mathrm{c}}\cos\beta\left[\frac{-6\,(x-x_0)^2\,(z-z_0)+2\,(z-z_0)^3}{r^6}\right] + \alpha_{\mathrm{c}}\sin\beta\left[\frac{-2\,(x-x_0)^3+6\,(x-x_0)\,(z-z_0)^2}{r^6}\right]. \tag{8}$$

In the case of a magnetic cylinder ($N = 2$), substituting equation (8) in the right-hand side of equation (2), we obtain

$$(x-x_0)\frac{\partial}{\partial x}\left(\frac{\partial M}{\partial z}\right) + (z-z_0)\frac{\partial}{\partial z}\left(\frac{\partial M}{\partial z}\right) = \alpha_{\mathrm{c}}\left\{\cos\beta\,\frac{[18(x-x_0)^2(z-z_0)-6(z-z_0)^3]}{r^6} - \sin\beta\,\frac{[6(x-x_0)^3+18(x-x_0)(z-z_0)^2]}{r^6}\right\}. \tag{9}$$

In the sense of least-squares, we can solve equation (9) for α_{c} and β. Moreover, we can determine the product of magnetization contrast and cross-sectional area (i.e. kFS).

TESTS ON SYNTHETIC DATA

To demonstrate the feasibility of the proposed method, we use simple 2D models as shown in Figs 1–5. The models consist of contacts, thin dikes, cylinders and two composite situations. For convenience, the magnetization intensity of models 1–4 is set at 5 A/m, and the magnetic declination and inclination are 10° and 30°, respectively. The grid spacing along the profile is 0.2 km.

Contact model (model 1)

The contact model is shown in Fig. 1(a) and its corresponding magnetic anomaly is shown in Fig. 1(b). Fig. 1(c) is the amplitude of the analytic signal of the first vertical derivative of the anomaly of Fig. 1(a). By using a Hilbert transform (Hsu *et al*. 1996), we can obtain the vertical and horizontal derivatives of Fig. 1(a). We can solve for the depths and structural index by using Euler's equation (equation 2). The three unknowns, x_0, z_0 and N, are to be determined. In general, three equations are sufficient to solve for three unknowns. We can overdetermine the three parameters, in the least-squares sense, to obtain more reliable solutions. In this study, every 16 consecutive data points along the profile are used to form the general equation. The results show that 'good' solutions cluster and converge at the real locations and structural indices, while the diffused solutions are deemed 'incorrect' (Figs 1c.e). Theoretically, a structural index is always greater than zero; the negative structural indices suggest wrong solutions which most often occur as a result of data inaccuracies and should be eliminated from the final results. For the contact model, depth solutions cluster at the top and edge of the model and structural-index solutions cluster near the value of zero. Good depth and structural-index solutions are at the same locations, where the

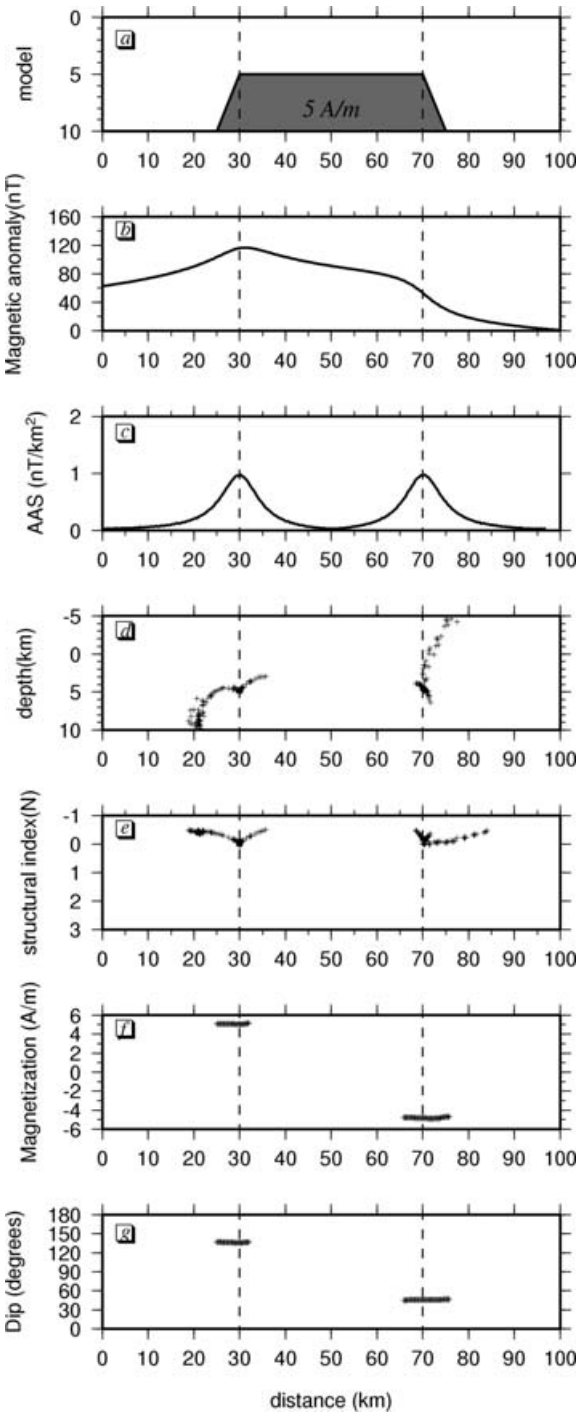

Figure 1 (a) Contact model geometry. (b) Magnetic anomaly caused by a contact structure. (c) Amplitude of the first-order analytic signal (*AAS*). (d) The calculated depth solutions. (e) The calculated structural index solutions. (f) Magnetization contrast of a contact model: left-hand-side solutions cluster at a value of 5 A/m; right-hand-side solutions cluster at a value of –5 A/m. (g) Contact model structural dips: left-hand-side solutions cluster at a value of 135°; right-hand-side solutions cluster at a value of 45°.

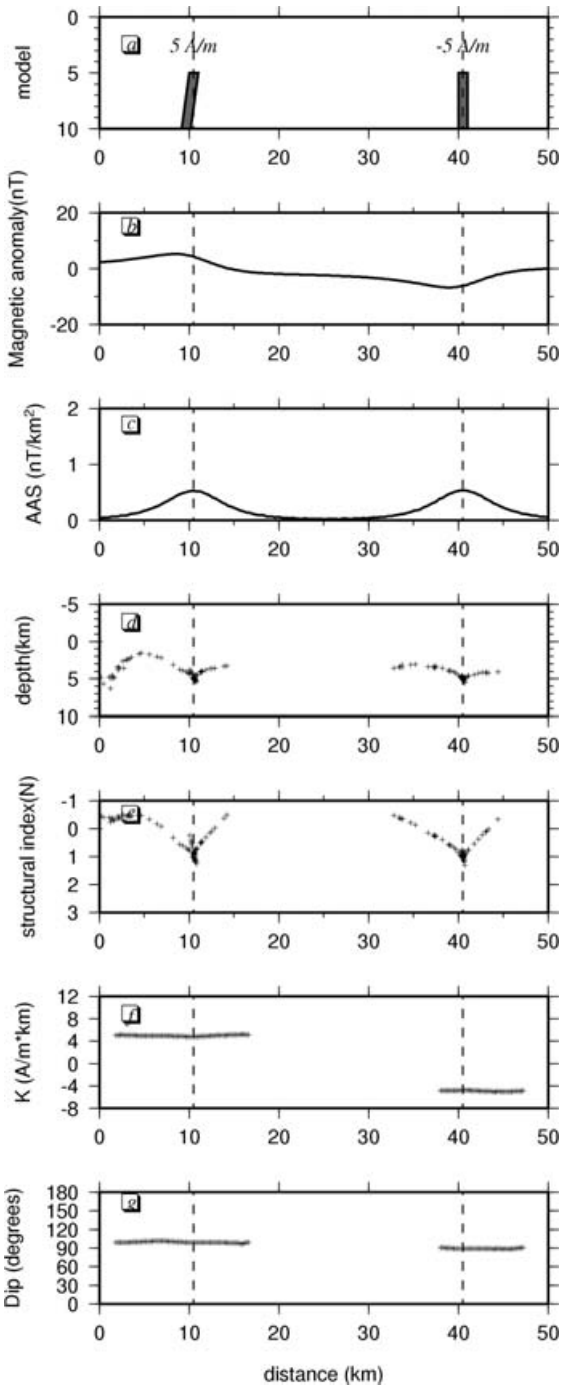

Figure 2 (a) Thin-dike model geometry. (b) Magnetic anomaly caused by two thin-dike structures. (c) Amplitude of the first-order analytic signal (*AAS*). (d) The calculated depth solutions. (e) The calculated structural index solutions. (f) The product of the magnetization contrast and thickness solutions (κ): left-hand-side solutions cluster at a value of 5 Am^{-1}km; right-hand-side solutions cluster at a value of –5 Am^{-1}km. (g) Thin-dike model structural dips: left-hand-side solutions cluster at a value of 100°; right-hand-side solutions cluster at a value of 90°.

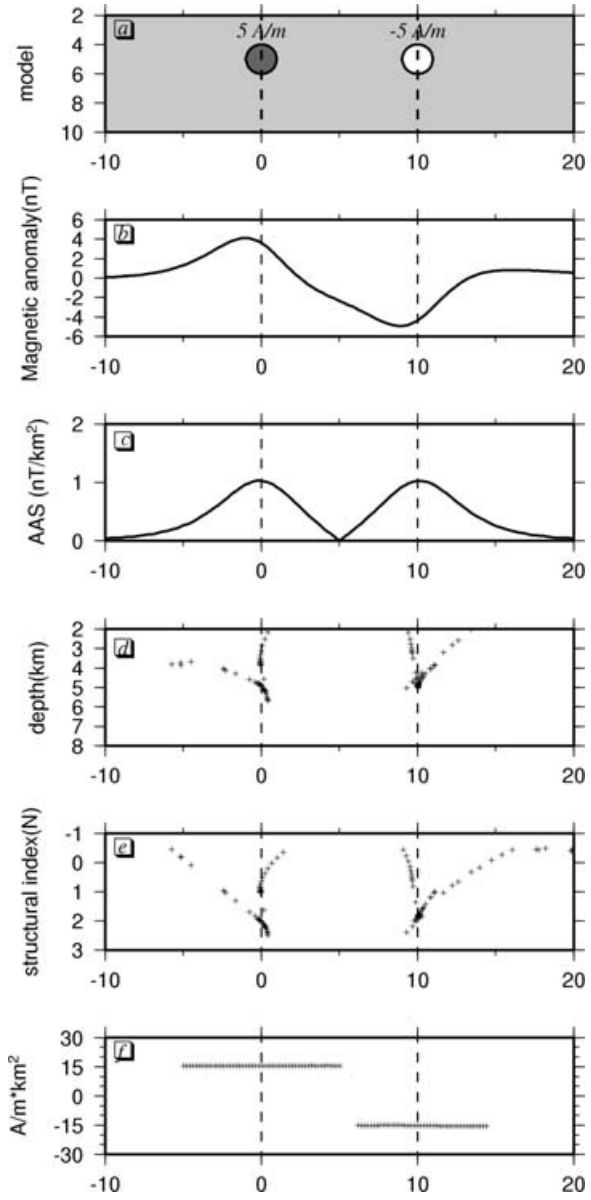

Figure 3 (a) Cylinder model geometry. (b) Magnetic anomaly caused by a cylinder structure. (c) Amplitude of the first-order analytic signal (*AAS*). (d) The calculated depth solutions. (e) The calculated structural-index solutions. (f) The product of the magnetization contrast and the cross-sectional area solutions (κ): left-hand-side solutions cluster at a value of 15.7 $Am^{-1}km^2$; right-hand-side solutions cluster at a value of –15.7 $Am^{-1}km^2$.

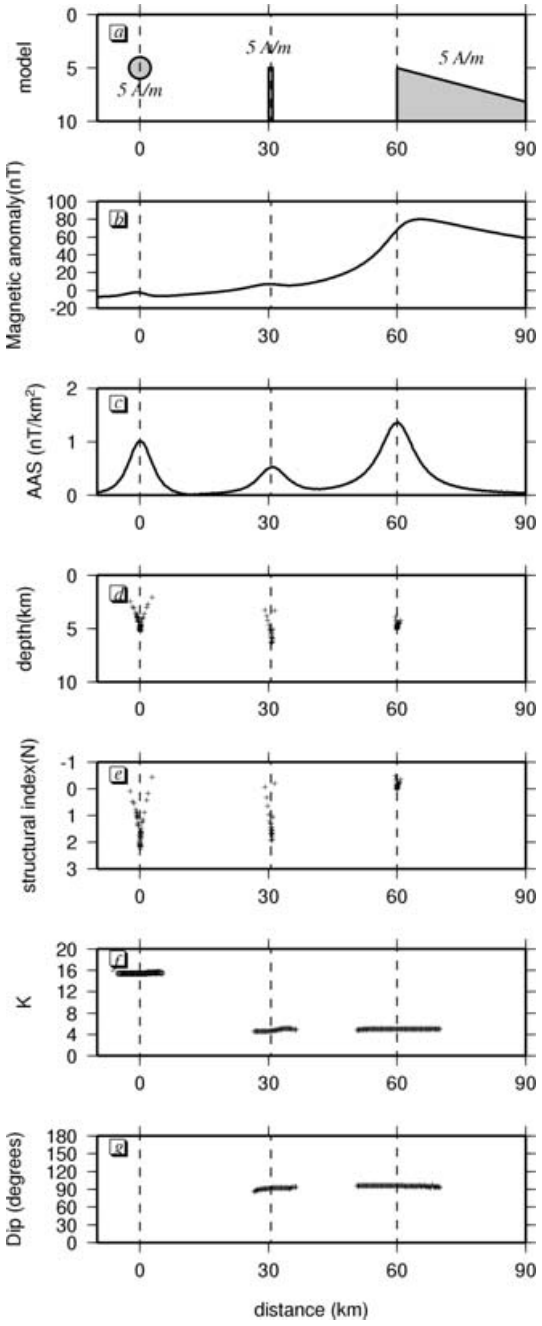

Figure 4 (a) Composite model geometry. (b) Magnetic anomaly caused by a composite model. (c) Amplitude of the first-order analytic signal (*AAS*). (d) The calculated depth solutions. (e) The calculated structural index solutions. (f) For the cylinder model, κ represents the product of the magnetization contrast and the cross-sectional area; solutions cluster at a value of 15.7 $Am^{-1}km^2$. For the thin-dike model, κ represents the product of the magnetization contrast and thickness; solutions cluster at a value of 5 $A/m^{-1}km$. For the contact model, κ represents the magnetization contrast; solutions cluster at a value of 5 A/m. (g) Structural dips: the solution for the thin-dike model is 90°; for the contact model the solution is 90°.

analytic signal displays maximum amplitudes (peaks) (Figs 1c.e). Using the analytic-signal technique, we can determine magnetic-source locations, while using Euler deconvolution, we can determine source depths and structural indices. Combining these two techniques can help us to image the depths

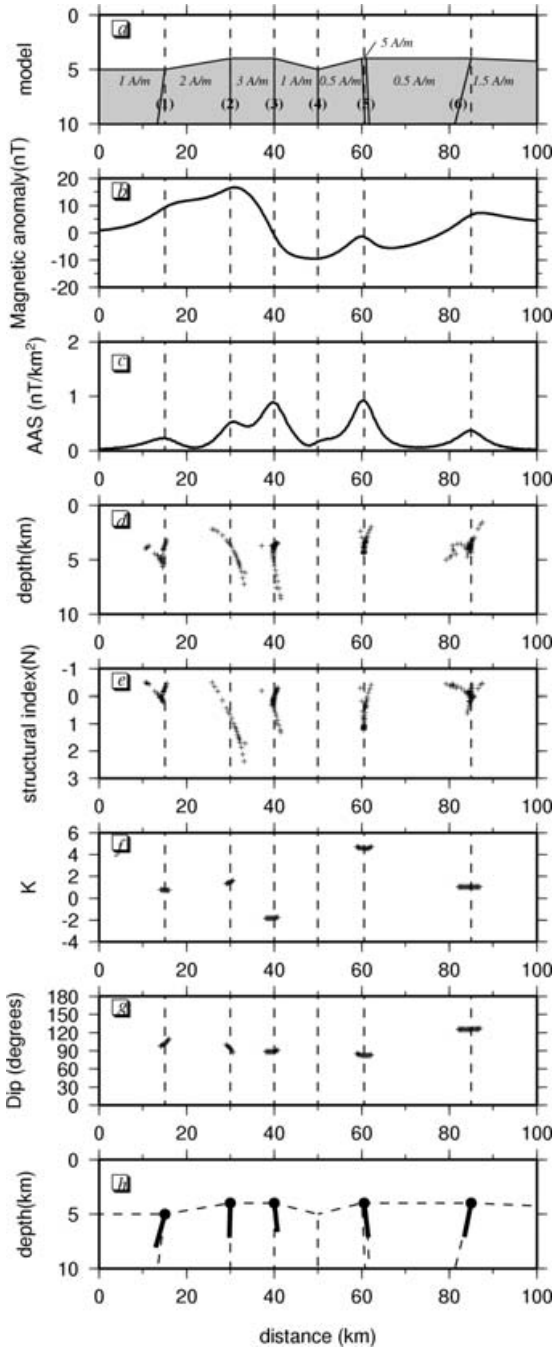

Figure 5 (a) Composite model geometry. (b) Magnetic anomaly caused by a composite model. (c) Amplitude of the first-order analytic signal (*AAS*). (d) The calculated depth solutions. (e) The calculated structural-index solutions. (f) Magnetization contrast (κ): this represents the magnetization contrast (A/m) when the structural index is equal to zero; when the structural index is equal to one, κ represents the product of the magnetization contrast and thickness. (g) Structural dips (degrees). (hours) Thick black lines indicate the directions of the calculated structural dips; dashed lines indicate the directions of the initial structural dips.

and types of the causative sources more precisely. Based on the source parameters obtained (x_0, z_0 and N) in Figs 1(d.e), we can solve for α ($\alpha = 2kFc\ \sin(d)$) and β ($\beta = 2I - d - 90^\circ$) by using equation (4). Furthermore, we can determine the structural dip and the magnetization contrast (Figs 1g.f), if we assume that the magnetization direction is the same as the present earth's magnetic field. The results show that the structural dip is about 135° and the magnetization contrast is about 5 A/m (Figs 1f.g and Table 2).

Thin-dike model (model 2)

The thin-dike model is shown in Fig. 2(a) and its corresponding magnetic anomaly is shown in Fig. 2(b). Fig. 2(c) is the amplitude of the analytic signal of the first vertical derivative of the anomaly of Fig. 2(a). Like the contact model, we can obtain the vertical and horizontal derivatives of Fig. 2(a), and solve for the depths and structural index using Euler's equation (equation 2). For the thin-dike model, depth solutions cluster at the top and centre of the model and structural-index solutions cluster around the value of one. Good depth and structural-index solutions are at the same locations, where the analytic signal has maximum amplitudes (peaks) (Fig. 2c–e). Using the same algorithm as in the contact model, we can determine x_0, z_0 and N. However, in the thin-dike model, we can determine the product of magnetization contrast and dike thickness by using equation (6). The results show that the structural dip is about 100° and the product of magnetization contrast and dike thickness is about 5 $Am^{-1}km$ (Figs 2f.g and Table 2).

Cylinder model (model 3)

The cylinder model is shown in Fig. 3(a) and its corresponding magnetic anomaly is shown in Fig. 3(b). Fig. 3(c) is the amplitude of the analytic signal of the first vertical derivative of the anomaly of Fig. 3(a). By using the vertical and horizontal derivatives of Fig. 3(a), we can solve for the source depths and structural index using Euler's equation (equation 2). As for the case of the contact model, we can determine x_0, z_0 and N. For the cylinder model, the good depth solutions cluster at the centre of the cylinder and good structural-index solutions cluster around the value of two. Good depth and structural-index solutions are at the same locations, where the analytic signal has maximum amplitudes (peaks) (Fig. 3c–e). Using the same procedure as for the contact model, we can determine x_0, z_0 and N. Based on the source parameters obtained (x_0, z_0 and N), we can solve for α ($\alpha_c = 2kF_0'S\frac{\sin i}{\sin i'}$) and β ($\beta = 2i' - 180^\circ$)

Table 2 Test models used in this study. S.D. standard deviation

Models	Magnetization contrast (A/m)	Dip (degrees)			
		Theoretical value	Estimated value	Theoretical value	Estimated value
		± 1 SD.		± 1 SD.	135.62 ± 0.38
Contact	Left	5.0	5.04 ± 0.03	135.0	45.71 ± 0.37
(model 1)	Right	–5.0	–4.84 ± 0.06	45.0	95.74 ± 1.01
Dike	Left	5.0	4.84 ± 0.11	96.28	89.52 ± 0.89
(model 2)	Right	–5.0	–4.98 ± 0.11	90.0	
Cylinder	Left	15.71	15.51 ± 0.18		
(model 3)	Right	–15.71	–15.47 ± 0.21		89.88 ± 0.83
Composite model	Contact	5.0	4.98 ± 0.04	90.0	91.27 ± 1.66
(model 4)	Dike	5.0	4.78 ± 0.21	90.0	–
	Cylinder	15.71	15.34 ± 0.19	–	106.24 ± 4.22
Composite model	1	1.0	0.75 ± 0.02	107.35	94.01 ± 4.31
(model 5)	2	1.0	1.46 ± 0.10	90.0	83.71 ± 0.83
	3	–2.0	–1.81 ± 0.03	90.0	failed
	4	–0.5	failed	90.0	82.84 ± 0.98
	5	4.5	4.62 ± 0.06	82.87	124.46 ± 0.51
	6	1.0	1.02 ± 0.01	122.85	

by using equation (9), and we can determine the product of magnetization contrast and cross-sectional area (Fig. 3f). The results show that the product of magnetization contrast and cross-sectional area is about 15.7 $Am^{-1}km^2$ (Fig. 3f and Table 2).

Composite models (models 4 and 5)

The first composite model, with three sources, is shown in Fig. 4(a). Its corresponding magnetic anomaly is shown in Fig. 4(b). Fig. 4(c) is the amplitude of the analytic signal of the first vertical derivative of the anomaly of Fig. 4(a). The peaks of analytic signals represent the structure boundaries or the centres of the structures. By using the vertical and horizontal derivatives of Fig. 4(a), we can solve for the depths and structural indices using Euler's equation (equation 2). In the sense of least-squares, we can determine x_0, z_0 and N. Good depth and structural-index solutions are at the locations where the analytic signal has maximum amplitudes (peaks) (Fig. 4c–e). Using joint analysis of the analytic-signal and Euler-deconvolution methods, we can obtain values of x_0, z_0 and N more accurately. For the first source, we use equation (9) because the structural index N is 2; for the second source, we use equation (6) because the structural index N is 1; for the third source, we use equation (4) because the structural index N is 0. We then determine the structural dip and the magnetization contrast using the relevant equations. The results are shown in Figs. 4(f.g).

The second composite model is more realistic, with six contrast sources (Fig. 5a). Its corresponding magnetic anomaly is shown in Fig. 5(b). Fig. 5(c) is the amplitude of the analytic signal of the first vertical derivative of the anomaly of Fig. 5(a). Using the vertical and horizontal derivatives of Fig. 5(a), we can solve for the depths and structural index (x_0, z_0 and N) by using the first derivative of Euler's equation (2). Good depth and structural-index solutions are at the same locations, where the analytic signal has maximum amplitudes (peaks) (Fig. 5c–e). However, each different structural index has its own appropriate equation to calculate dip and magnetization contrast. For the first, second, third, sixth sources, we use equation (4), because their structural indices are near to zero. However, for the fifth source, we use equation (6), because the structural index is close to one. We can then determine the structural dip and magnetization contrast. The structural dip is defined as the angle taken in a clockwise direction from the positive x-direction; it varies from 0° to 180°. We show the modelling results and true model values in Table 2. For the fourth source, the analytic signal does not have a clear maximum amplitude, so we cannot identify the correct structural source position. The results are shown in Fig. 5 and Table 2.

REAL EXAMPLE

To demonstrate the feasibility of the proposed method, we analyse a magnetic profile across the Formosa Canyon, off

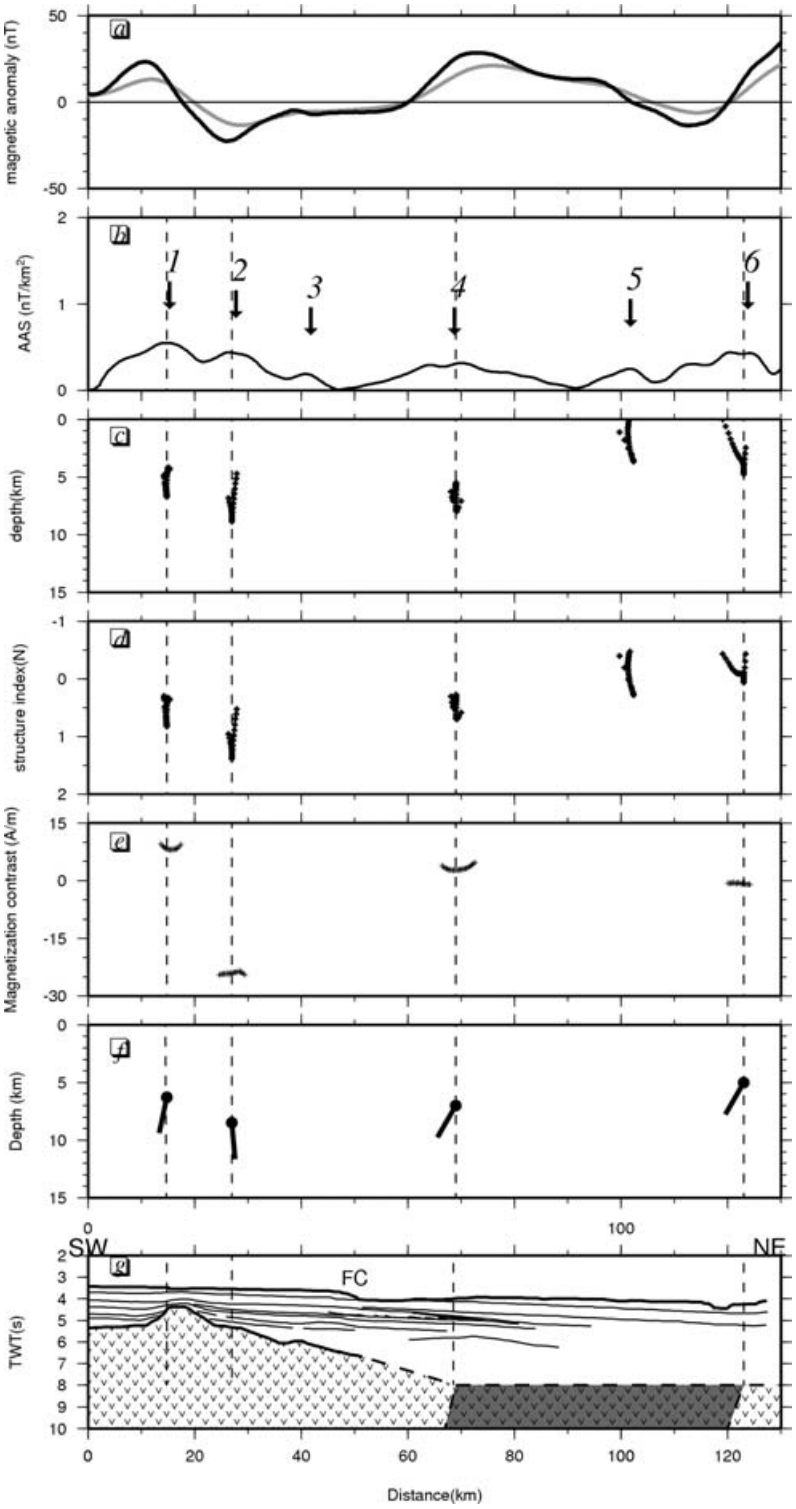

Figure 6 (a) Magnetic anomaly of real data; the black line indicates the total magnetic anomaly and the grey line indicates the 3 km upward continuation of the anomaly. (b) Amplitude of the first-order analytic signal (*AAS*). (c) The calculated depth solutions. (d) The calculated structural index solutions. (e) Magnetization contrast: this represents the magnetization contrast (A/m) when the structural index is equal to zero; it represents the product of the magnetization contrast and thickness when the structural index is equal to one. (f) Structural dips (degrees); thick black lines indicate the directions of the calculated structural dips. (g) An interpreted seismic profile along the magnetic profile (Yeh and Hsu 2004), including the interpreted zone (dark grey zone) inferred from the magnetic result. FC: Formosa Canyon. The dashed line is the interpreted top of the volcanic basement.

south-west Taiwan (Hsu *et al*. 2004; and Yeh and Hsu 2004). Based on previous seismic and magnetic interpretations, the location of the Formosa Canyon shows a bathymetric escarpment. Although it has been suggested that the Formosa Canyon is the location of a basement discontinuity (Hsu *et al*. 2004; Yeh and Hsu 2004), the seismic profile could only identify the volcanic basement along the distance 0–50 km (Fig. 6g). For this real data, several different data windows were tried in order to obtain the best depth and structural-index solutions (Figs 6c.d). Figs 6(c.d) shows that good depth and structural-index solutions are placed at the locations where the analytic signal generally displays maximum amplitudes (peaks). Comparing the *AAS* and the Euler equation results, we can identify four meaningful solutions (numbers 1, 2, 4 and 6, located at 15 km, 28 km, 69 km and 123 km, respectively) in Fig. 6. The depth solutions are 6.3 km, 8.5 km, 7.1 km and 4.8 km, respectively, and the structural-index solutions are 0.83, 1.12, 0.35 and 0.05, respectively. For a simple geological interpretation, we assume that the structural indices are 1, 1, 0 and 0, i.e. close to the four solutions. In fact, the location of solution number 1 indicates the existence of a volcanic intrusion buried at 4.5 s TWT (two-way traveltime). This structure is considered to be a dike-dike structure. In that case, we can solve for magnetization contrast (the product of the magnetization contrast and thickness) by using equation (6) and the result is 8.23 Am^{-1}Km; in the same way, the solution of the structural dip is equal to 102.2°. According to our results, there is no solution directly beneath the Formosa Canyon. However, we do find a solution slightly further from the location of the Formosa Canyon (solution number 4) (Fig. 6). It could be interpreted as a step-dike structure. In that case, the solution of the magnetization contrast is 3.42 Am^{-1} and the structural dip is 120.2°. Thus, based on the magnetic anomaly analysis, a major structural boundary, dipping to the south at an approximate distance of 70 km is indicated. This implies that the corresponding basement has higher magnetization than the southern volcanic zone (Fig. 6g).

CONCLUSION

We propose an interpretational approach using the analytic signal and Euler deconvolution to estimate the magnetic-source parameters of a 2D contact, a thin dike and a cylinder. The major advantage of using a joint analysis is that not only can we determine the depths and possible geometric types (structural indices) of magnetic sources, but we can also estimate structural dips and magnetization contrast. The synthetic models show that the feasibility of the proposed method is quite good. However, if the magnetic interference between two adjacent structures is too large, the method fails to solve the magnetic parameters. The maximum amplitudes (peaks) of the analytic signal in the 2D profile can also be used as an auxiliary method for judging the existence of probable solutions at the same locations. In real data, the structural index of a simple 2D model must be assigned for further estimation of the magnetization contrast and structural dip of the model.

ACKNOWLEDGEMENTS

The comments and suggestions from editor, Dr Alan Reid, and two anonymous reviewers are appreciated. This study was carried out with grants from the Central Geological Survey and the National Science Council of Taiwan.

REFERENCES

Fedi M. and Florio G. 2001. Detection of potential field source boundaries by enhanced horizontal derivation method. *Geophysical Prospecting* **49**, 40–58.

Hsu S.-K. 2002. Imaging magnetic sources using Euler's equation. *Geophysical Prospecting* **50**, 15–25.

Hsu S.-K., Coppens D. and Shyu C.-T. 1998. Depth to magnetic source using the generalized analytic signal. *Geophysics* **63**, 1947–1957.

Hsu S.-K., Sibuet J.-C. and Shyu C.-T. 1996. High-resolution detection of geologic boundaries from potential-field anomalies: an enhanced analytic signal technique. *Geophysics* **61**, 373–386.

Hsu S.-K., Yeh Y.-C., Doo W.-B. and Tsai C.-H. 2004. New bathymetry and magnetic lineation identifications in the northernmost South China Sea and their tectonic implications. *Marine Geophysical Researches* **25**, 29–44.

Murthy K.S.R. and Mishra D.C. 1980. Fourier transform of the general expression for the magnetic anomaly due to a long horizontal cylinder. *Geophysics* **45**, 1091–1093.

Mushayandebvu M.F., van Driel P., Reid A.B. and Fairhead J.D. 2001. Magnetic source parameters of two-dimensional structures using extended Euler deconvolution. *Geophysics* **66**, 814–823.

Nabighian M.N. 1972. The analytic signal of two-dimensional magnetic bodies with polygonal cross-section: its properties and use for automated anomaly interpretation. *Geophysics* **37**, 507–517.

Nabighian M.N. 1974. Additional comments on the analytic signal of two-dimensional magnetic bodies with polygonal cross-section. *Geophysics* **39**, 85–92.

Nabighian M.N. 1984. Toward a three-dimensional automatic interpretation of potential field data via generalized Hilbert transforms: fundamental relations. *Geophysics* **49**, 957–966.

Ravat D. 1996. Analysis of the Euler method and its applicability in environmental magnetic investigations. *Journal of Environmental and Engineering Geophysics* **1**, 229–238.

Reid A.B., Allsop J.M., Granser H., Millett A.J. and Somerton I.W. 1990. Magnetic interpretation in three dimensions using Euler deconvolution. *Geophysics* **55**, 80–91.

Roest W.R., Verhoef J. and Pilkington M. 1992. Magnetic interpretation using the 3-D analytic signal. *Geophysics* **57**, 116–125.

Salem A. and Ravat D. 2003. A combined analytic signal and Euler method (AN-EUL) for automatic interpretation of magnetic data. *Geophysics* **68**, 1952–1961.

Smith R.S. and Salem A. 2005. Imaging depth, and susceptibility from magnetic data: The advanced source-parameter imaging method. *Geophysics* **70**, 31–38.

Smith R.S., Thurston J.B., Dai T.-F. and MacLeod I.N. 1998. iSPI^{TM} – the improved source parameter imaging method. *Geophysical Prospecting* **46**, 141–151.

Thompson D.T. 1982. EULDPH: a new technique for making computer-assisted depth estimates from magnetic data. *Geophysics* **47**, 31–37.

Thurston J.B. and Smith R.S. 1997. Automatic conversion of magnetic data to depth, dip, and susceptibility contrast using the SPI (TM) method. *Geophysics* **62**, 807–813.

Williams S.E., Fairhead J.D. and Flanagan G. 2005. Comparison of grid Euler deconvolution with and without 2D constraints using a realistic 3D magnetic basement model. *Geophysics* **70**, 13–21.

Yeh Y.-C. and Hsu S.-K. 2004. Crustal structures of the northernmost South China Sea: Seismic reflection and gravity modeling. *Marine Geophysical Researches* **25**, 45–61.